## **Zhe Chen**

State Key Laboratory of Fluid Power and Mechatronic System, Key Laboratory of Soft Machines and Smart Devices of Zhejiang Province, Department of Engineering Mechanics, Zhejiang University, Hangzhou 310027, China

## Tonghao Wu

State Key Laboratory of Fluid Power and
Mechatronic System,
Key Laboratory of Soft Machines and Smart
Devices of Zhejiang Province,
Department of Engineering Mechanics,
Zhejiang University,
Hangzhou 310027, China

# **Guodong Nian**

State Key Laboratory of Fluid Power and Mechatronic System, Key Laboratory of Soft Machines and Smart Devices of Zhejiang Province, Department of Engineering Mechanics, Zhejiang University, Hangzhou 310027, China

## Yejie Shan

State Key Laboratory of Fluid Power and Mechatronic System, Key Laboratory of Soft Machines and Smart Devices of Zhejiang Province, Department of Engineering Mechanics, Zhejiang University, Hangzhou 310027, China

# Xueya Liang

State Key Laboratory of Fluid Power and Mechatronic System, Key Laboratory of Soft Machines and Smart Devices of Zhejiang Province, Department of Engineering Mechanics, Zhejiang University, Hangzhou 310027, China

# Hanging Jiang<sup>1</sup>

School for Engineering of Matter, Transport and Energy, Arizona State University, Tempe, AZ 85287 e-mail: Hanqing.Jiang@asu.edu

# Shaoxing Qu<sup>1</sup>

State Key Laboratory of Fluid Power and Mechatronic System, Key Laboratory of Soft Machines and Smart Devices of Zhejiang Province, Department of Engineering Mechanics, Zhejiang University, Hangzhou 310027, China e-mail: squ@zju.edu.cn

# Ron Resch Origami Pattern Inspired Energy Absorption Structures

Energy absorption structures are widely used in many scenarios. Thin-walled members have been heavily employed to absorb impact energy. This paper presents a novel, Ron Resch origami pattern inspired energy absorption structure. Experimental characterization and numerical simulations were conducted to study the energy absorption of this structure. The results show a new collapse mode in terms of energy absorption featuring multiple plastic hinge lines, which lead to the peak force reduction and larger effective stroke, as compared with the classical honeycomb structure. Overall, the Ron Resch origami-inspired structure and the classical honeycomb structure are quite complementary as energy absorption structures. [DOI: 10.1115/1.4041415]

Keywords: absorber, origami, finite element simulation, 3D printing

<sup>&</sup>lt;sup>1</sup>Corresponding authors.

Contributed by the Applied Mechanics Division of ASME for publication in the JOURNAL OF APPLIED MECHANICS. Manuscript received August 16, 2018; final manuscript received September 4, 2018; published online October 5, 2018. Editor: Yonggang Huang.

#### 1 Introduction

Energy absorption structures [1] that deform and absorb kinetic energy during impact have been widely utilized to enhance the crashworthiness in various situations, including vehicles [2-5], crash barriers [6], nuclear reactors [7], and bridges [8]. Thinwalled members (or tubular structures) with circular or square cross section have been heavily used to absorb energy under axial loading [9–15]. Tubes with other cross-sectional shapes, including pentagonal tubes, hexagonal tubes, and some prefolded surface tubes [16–21], have also been studied for their crashworthiness performance. In addition to tubes, the composite sandwich structure consisting of a lighter core material sandwiched between two stiffer sheets is also adopted as a primary energy absorption structure in several industrial sectors because of its low-weight and high-energy absorbability [22-24] in which the stiffer sheet enables even distribution of loads over the lighter core materials. Despite different structures being used, the mechanisms of energy absorption mainly come from three sources [12], i.e., (1) folding along stationary plastic hinge lines, (2) propagation of traveling plastic hinge lines, and (3) localized in-plane stretching. For crashing structure with square and circular cross section, among these three contributions, in-plane extensional deformation occurs only at very small fraction of the total area of the shell but contributes as much as one-third of the total energy dissipated in the structure; while the other two mechanisms, stationary and moving plastic hinge lines, contribute another two-thirds of the absorbed energy [12]. Significant efforts have been focused on the energy absorption characteristics, i.e., the crushing mode when a thinwalled structure is subjected to axial load [11,13,14]. The common modes are symmetric mode, nonsymmetric diamond mode, or a mix of these two [20].

Although the design requirements may vary notably from one application to another, some fundamental principles exist for all applications [17]. The main ones are (1) low peak reaction force  $F_{\text{peak}}$  of an energy absorber to prevent excessive force being transmitted to the main structure during the crushing process, (2) high mean crushing force  $F_{\text{mean}}$  that is defined as the integral mean of the crushing force F(x) within the range of the effective stroke H, i.e., total energy absorption within the range of the effective stroke H divided by H

$$F_{\text{mean}} = \frac{\int_0^H F(x)dx}{H} \tag{1}$$

To determine the effective stroke H, a variable named "deformation efficiency f" was introduced [25]

$$f(s) = \frac{\int_0^s F(x)dx}{F_{\text{max}}(s)} \tag{2}$$

where s is the crush distance and  $F_{\rm max}$  is the maximum crush force in crush process [0,s], except peak force  $F_{\rm peak}$ . When the deformation efficiency f(s) reaches a maximum at a certain s, the corresponding crushing distance s is thus the effective stroke H. A common method to reduce the peak force  $F_{\rm peak}$  is to introduce some imperfections in absorption structures, such as dents [26] or prefolded pattern [20]. Adding cross-sectional area or applying ribs as stiffeners [27] can increase the mean crushing force  $F_{\rm mean}$ . In addition to the peak force and mean crushing force, many other quantities have been introduced to evaluate the energy absorption capacity, such as the specific energy absorption defined as energy absorption capacity per unit mass, and the load uniformity defined as the ratio of the peak force to the mean crushing force.

Recently, origami, the art of paper folding that creates 3D structures from 2D sheets through a high degree of folding along the creases, has been explored to create new energy absorption structures [20,21,28–36], in addition to mechanical metamaterials

[37–39] and foldable structure applying in space exploration [40]. Since the origami patterns are made from 2D sheets, the 3D folded pattern is developable, and thus, can be readily manufactured. The main rationale of adopting origami structures as energy storage is to utilize the predefined crease lines to control the crushing mode. In other words, the origami structure would follow the origami pattern during a crash, and thus, the crushing mode is determined by the predefined pattern. Specifically, for the fundamental principles on the design of energy absorption structures, namely, low peak reaction force and high mean crushing force, the crease lines that are perpendicular to the axial direction would function as the grooves to reduce the peak force. Meanwhile, these crease lines may also function as the traveling plastic hinge lines, one of the three mechanisms to dissipate energy.

In this paper, we study the energy absorption capability of a particular origami pattern, namely Ron Resch pattern, and its derivatives. 3D printing is used to prepare the sample for crushing. The experimental and finite element simulation results are compared and analyzed.

#### 2 Rationale of Choosing the Ron Resch Pattern

A Ron Resch origami pattern is shown in Fig. 1(a). The solid lines represent "mountain" creases that will remain on the top after folding and the dashed lines are for the "valley" creases that will stay on the bottom after folding. Gradually folding a paper along the creases, the Ron Resch pattern in a dome shape is shown in Fig. 1(b). After that, a Ron Resch dome can be transformed into a flat state (namely, a Ron Resch plate) when applying the compressive load on top of the dome. Three dihedral angles,  $\beta_1$ ,  $\beta_2$ , and  $\beta_3$ , are used to describe this origami folding (Fig. 1(c) [37]). When  $\beta_1 = \beta_2 = \beta_3 = 180 \deg$ , it describes a planar state (Fig. 1(a)). When  $\beta_1 \in [0 \deg, 180 \deg]$ ,  $\beta_2 \in [0 \deg, 180 \deg]$ , and  $\beta_3 \in [0 \deg, 180 \deg]$ , it represents a curved state (illustrated by the left inset of Fig. 1(b) [37]). When  $\beta_1 = 0 \deg, \beta_2$ = 120 deg, and  $\beta_3$  = 90 deg, it forms another planar state, i.e., Ron Resch plate state, illustrated by the right inset of Fig. 1(b). This more compact Ron Resch plate state shows a striking load bearing capability [37]. The energy absorbing structure shown in Fig. 1(d) is constructed using the Ron Resch plate. Two geometric parameters define the energy absorbing structure: the base line length l and the height h. In the original Ron Resch structure, the ratio of the *l* to the *h* is constant  $(l/h = \sqrt{3})$ . In this study, we aim to optimize the energy absorption capability; such that different land h ratios are used, i.e., Ron Resch inspired structures are studied.

The rationale of choosing the Ron Resch pattern as an object to study energy absorption is the following. During an axial crushing, the absorber usually exhibits three stages: an initial buckling stage, responsible for initial peak force; a plateau state which is caused by the plastic buckling and the progressive folding; finally, a densification stage due to the compaction of materials [25]. Plastic dissipation of the second stage is responsible for the majority of the total energy absorption. Wierzbicki and Abramowicz [12] presented that the energy dissipation came from folding along stationary plastic hinge lines, propagation of traveling plastic hinge lines, and localized in-plane stretching. Given that the Ron Resch structure consists of many triangles and triangles may generate many plastic hinge lines with different length at the post-buckling state when applying an axial crushing, it is thus assumed that the Ron Resch inspired structures could reduce the initial peak force as incipient buckling appearing relatively easily. And subsequent post-buckling would absorb more energy, thereby increasing mean crushing force.

# 3 Fabrication and Experimental Procedure of the Ron Resch Patterns

Three-dimensional printing provides a facile and low-cost approach to fabricate complex 3D objects, such as the Ron Resch

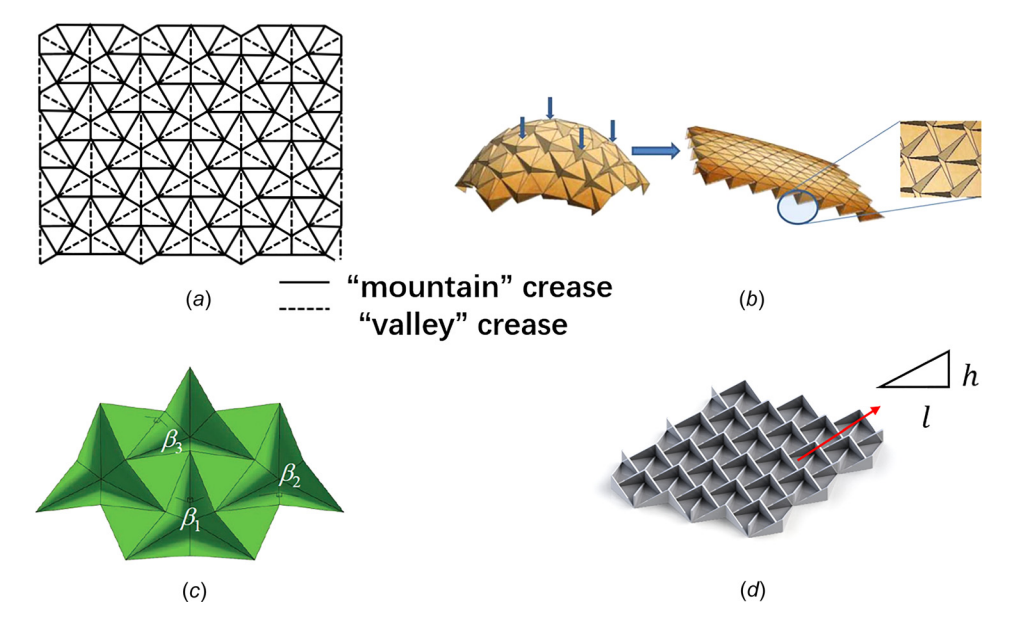


Fig. 1 Design of the origami energy absorber. (a) A Ron Resch pattern in its planar state. The solid lines represent "mountain" creases and the dashed lines represent "valley." (b) Process of a Ron Resch dome deforming to a Ron Resch plate upon compressive load from the top. (c) Three dihedral angles  $\beta_1$ ,  $\beta_2$ , and  $\beta_3$  are used to describe a Ron Resch pattern. (d) An energy absorbing structure with Ron Resch pattern. Two crucial geometric parameters I and I0 are used to describe the structure.

structure. Here, we choose an elastic-plastic 3D printing material-Nylon and selective laser sintering method (TPM3D S360) to fabricate the Ron Resch inspired structures. Illustration shown in Fig. 1(d) is used to 3D print the origami-inspired structures with chopped sharp corners of the triangles to avoid excessive stress concentration under compressive load. Figure 2(a) shows one specimen. The structure is composed of a core with Ron Resch plate pattern sandwiched between two sheets. The height (h) and the thickness (t) of the specimens are 11mm and 1mm, respectively. Three different sets of base line (1) are printed, with l = 11 mm, 20 mm, and 33 mm. The testing processes are shown in Fig. 2(b) and Supplemental Video S1 which is available under the "Supplemental Data" tab for this paper on the ASME digital collection. The axial crushing tests are conducted on a universal testing machine (SUNS 300KN). In the test, an absorber stands on a thick plate and the indenter moves downward to compress the structure. The velocity of compress is chosen as 5 mm/min for a quasi-static loading. When the structure reaches the compaction stage, i.e., the force appears a sharp rise, the test will be stopped. The experiment is repeated three times for each model. The curves for reaction force (F) versus displacement (s) will be recorded. The peak force  $F_{\text{peak}}$  and the mean crushing force  $F_{\text{mean}}$ of each structure are extracted from the experimental results.

Uniaxial tensile tests are conducted on the three tensile specimens which are fabricated by 3D printing using the identical material in axial crushing experiment at 5 mm/min loading rate to characterize the material properties. The average mechanical properties obtained are Young's modulus  $E=700\,\mathrm{Mpa}$ , yield stress  $\sigma_y=8\,\mathrm{MPa}$ , tensile strength  $\sigma_u=30.8\,\mathrm{Mpa}$ , and ultimate strain  $\varepsilon_u=14.8\%$ . And the engineering stress versus strain curve is plotted in Fig. 2(c). In addition, the density and Poisson's ratio of both materials are  $\rho=1080\,\mathrm{Kg/m^3}$  and  $\nu=0.3$ .

## 4 Finite Element Modeling

A periodic repeated unit of a Ron Resch inspired structure with different geometries is adopted to investigate the collapse mode and energy absorption properties. To compare with the experiments, the numerical models have the identical sizes as those in the experiments. In the simulations, the bottom plate of the absorber structure is constrained completely, and the upper one is tied to the moving rigid plate in all directions except the translational one in the axial direction (shown in Fig. 3(a)). Periodic boundary conditions are adopted on the peripheral boundaries of the finite element model. Imperfections are introduced in order to simulate the post-buckling behavior, such that the mode shapes of

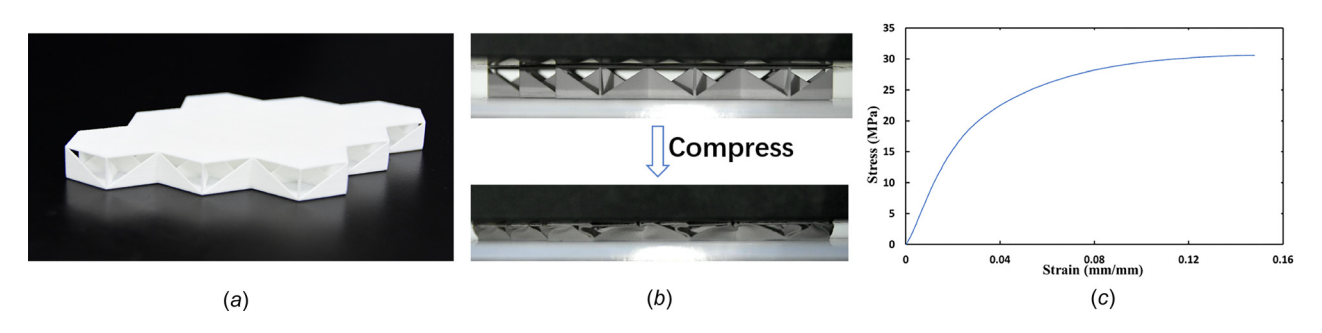


Fig. 2 Experiments for investigating the energy absorption properties of the origami absorber. (a) An origami absorber with multiple origami units is fabricated by 3D printing. (b) A quasi-static axial crushing test is carried out. (c) Material engineering stress-strain curve obtained by uniaxial tensile tests.

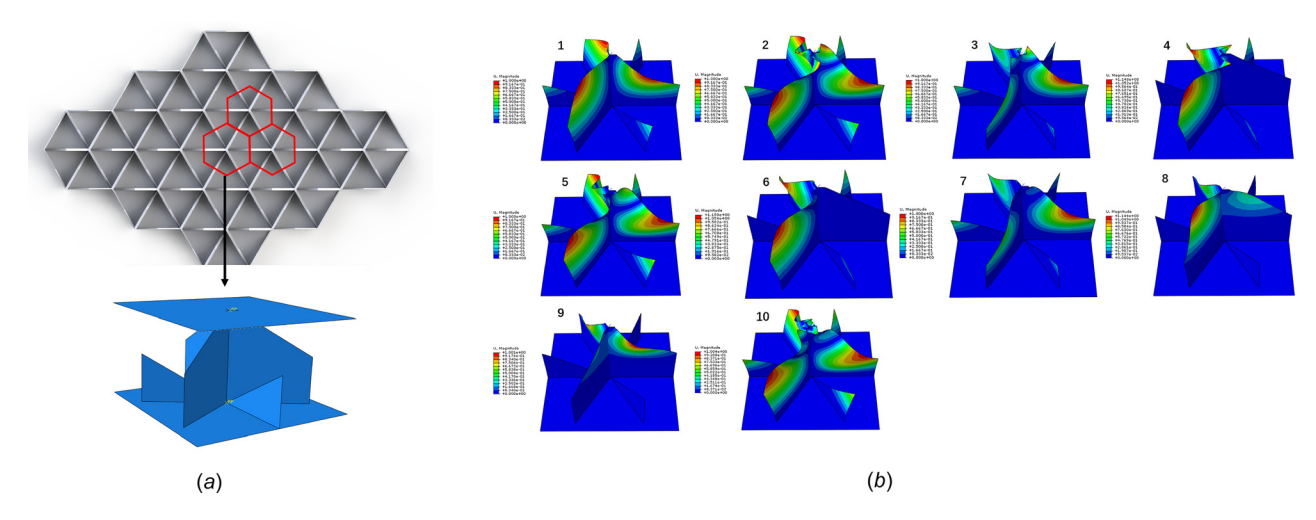


Fig. 3 (a) Setting up a numerical model. A periodic repeated unit of the origami absorber is adopted and the way to divide the periodic boundary is shown in the inset. (b) Ten natural modes of the numerical model.

the origami energy absorber, extracted via the mode analysis, are adopted as the imperfection. Figure 3(b) shows the first ten mode shapes for a structure with periodic repeated features of Ron Resch pattern. The finite element analysis software package ABAQUS/BUCKLE is used. Amplitudes of imperfections are distributed randomly in the range of 0.001-0.01. After introducing imperfections, post-buckling of absorber structure can proceed. Then, ABAQUS/EXPLICIT is applied for the post-buckling analysis. The scenario of post-buckling stage is similar to the prior one, but compression displacement is set to 80% of the height of the structure, h. Specified vertical displacement of the rigid plate is used to control the crushing process, and a smooth loading versus time curve is adopted to help numerical convergence. The smooth amplitude built in ABAQUS, which settles zero loading speed both at beginning and at the end of loading process to prevent mutation of loading speed, is assigned to the displacement of the moving rigid plate. The structure is mainly meshed of quadrilateral elements with reduced integration S4R, supplemented by a few triangular elements for avoiding excessive distortion. General contact is employed. Given that the 3D printed experimental specimen is composed of nylon powder by laser sintering and thus has a rough surface, friction is taken into consideration in the simulations with friction coefficient of  $\mu = 0.8$ . The Nylon used for 3D printing specimens is chosen as the material and mechanical properties have been provided in Sec. 3.

It must be noted that the axial crushing process in experiment is quasi-static, such that the ABAQUS/STANDARD solver that is designed

to deal with static problems should be applied. However, the crushing process involves extensive contact and local buckling, which is very challenging to solve using ABAQUS/STANDARD solver. Hence, the ABAQUS/EXPLICIT solver that is designed to solve dynamic problems is used to simulate the quasi-static process. Thus, a proper time-step in ABAQUS/EXPLICIT must be chosen. This time-step needs to be long enough to simulate a quasi-static state but also as short as possible with reasonable computational cost. In the simulations, we ensure that the ratio of the kinetic energy to the internal energy is below 5% to make the dynamic effect ignorable, and the ratio of artificial energy to internal energy is less than 5% to diminish the hourglass effect. The mesh density and analysis time should meet convergence requirements. Given the above, a global mesh size of 0.2 mm and an analysis time of 0.2 s are adopted.

#### 5 Results

Figure 4(a) shows the simulation results of the crushing process of a periodic repeated unit with l/h = 1.81, and the corresponding equivalent plastic strain (i.e., PEEQ used in ABAQUS) contour maps on undeformed shape for clarity are plotted in Fig. 4(b). Supplementary Video S2 which is available under the "Supplemental Data" tab for this paper on the ASME digital collection shows the dynamic compression process. About 10,448 S4R elements are employed and the  $0.2 \, \mathrm{s}$  analysis time is simulated. At the beginning ( $t = 0.045 \, \mathrm{s}$ ), the plastic strain takes place at the

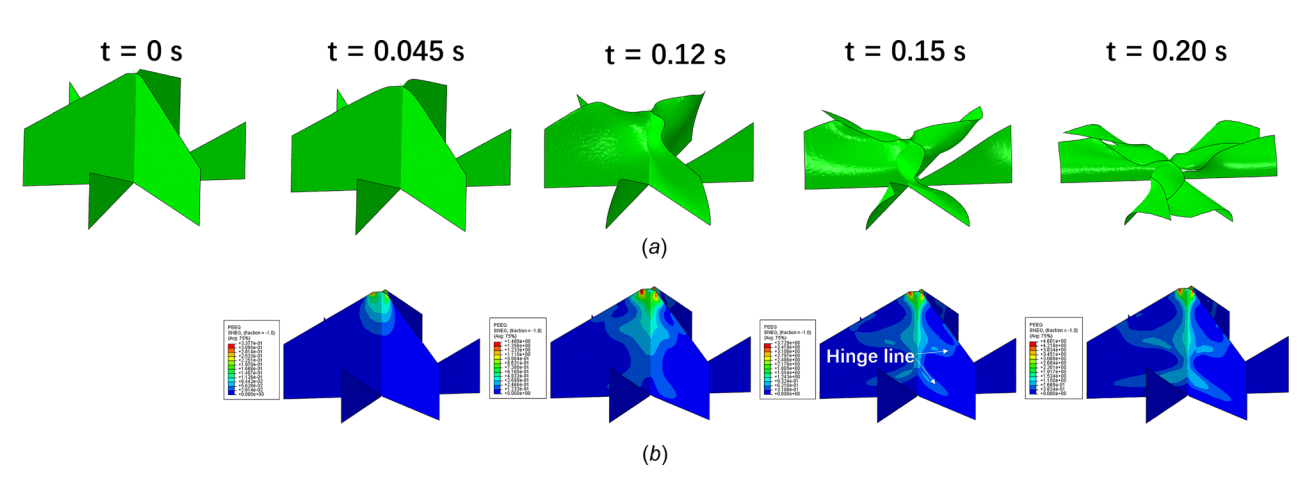


Fig. 4 (a) Crushing process of No. 2 model in simulation and (b) PEEQ contour maps. Here, No. 2 model represents the model with l/h = 1.81 shown in Table 1.



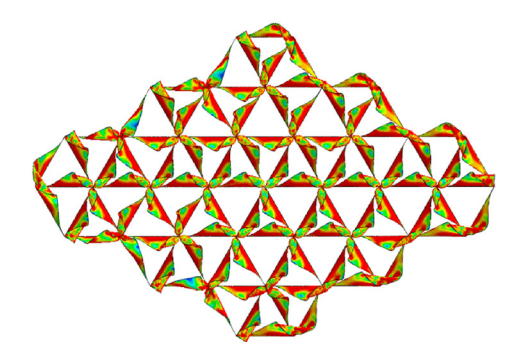
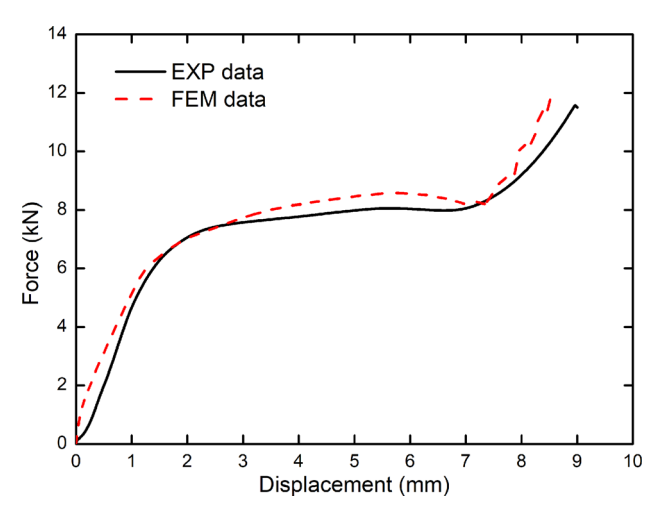


Fig. 5 Comparison of collapse mode in both experiment and simulation



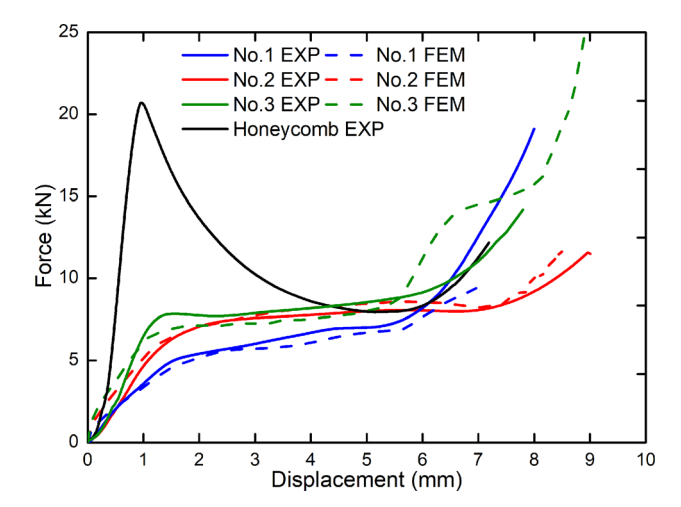


Fig. 6 Force versus displacement curves of No. 2 model obtained by both experiment and simulation. Here, No. 2 model represents the model with l/h = 1.81 shown in Table 1.

Fig. 7 Force versus displacement curves of physical and numerical models. Here, numbers 1, 2, 3 represent models with different *l* and *h* ratios shown in Table 1.

upper corner (Fig. 4(b)), close to the moving rigid plate, and propagates to the bottom of the structure along the central line. The configurations (t = 0.15 s) in Figs. 4(a) and 4(b) show the formation of two plastic hinge lines in each thin-wall, such that the thinwalls start to fold along plastic hinge lines. The PEEQ contour map in Fig. 4(b) at time t = 0.15 s clearly indicates that the large plastic deformation occurs around plastic hinge lines. As the structure is further compressed, the plastic strain along central line continues to propagate, and the plastic hinge lines become more apparent. The simulation completes when the elements have excessive distortion and the model is not completely flattened (time t = 0.2 s). At this state, three central thin-walls are folded along the horizontal plastic hinge, and the external three triangles also bend. Figure 5 shows the top view of the simulated origami absorber, which has great consistency with the experimental observation.

The force versus displacement curves of this model both in experiment and simulation are plotted in Fig. 6. Overall, the experiment and simulation fit very well. Supplementary Video S1 which is available under the "Supplemental Data" tab for this paper on

the ASME digital collection shows the dynamic compression process from the experiment. As it shows, the thin wall starts from linear bending before buckling at approximate time  $t=12\,\mathrm{s}$ , corresponding to the experimental curve before 1.5 mm in displacement. After that, the thin walls are folded and a smooth plateau with a maximum force around 8 kN presents. When crushing displacement reaches approximately 7.3 mm, the curve increases sharply due to self-contact. Based on Eqs. (1) and (2), the mean crushing force  $F_{\text{mean}}$ , the effective stroke H, and the energy absorption efficiency are calculated,  $F_{\text{mean}}=6.9\,\mathrm{kN}$  (experiemnts),  $F_{\text{mean}}=7.2\,\mathrm{kN}$  (simulations),  $H=7.7\,\mathrm{mm}$  (experiments),  $H=7.3\,\mathrm{mm}$  (simulations), which again show good agreement between experiments and simulations.

To optimize the origami geometry for energy absorption, two more structures with l/h=1 and 3 are studied. The force versus displacement curves are provided in Fig. 7 and Table 1 summarizes the key characteristics. With the decreasing of l/h=3 ratio (from 3 to 1), the structures become denser because the unit cell occupies smaller volume and the effective density increases. This

Table 1 Origami absorber geometries and numerical results

No.	l/h	Relative density	Effective stroke (mm)	$F_{\text{mean}}(\mathbf{K}\cdot\mathbf{N})$	Energy absorption efficiency (energy/volume) (J/cm³)
1	1	0.159	5.7	5.1	8.0
2	1.81	0.089	7.3	7.1	4.6
3	3	0.054	8.2	8.8	2.3
Honey-comb		0.089	5.9	10.6	5.4

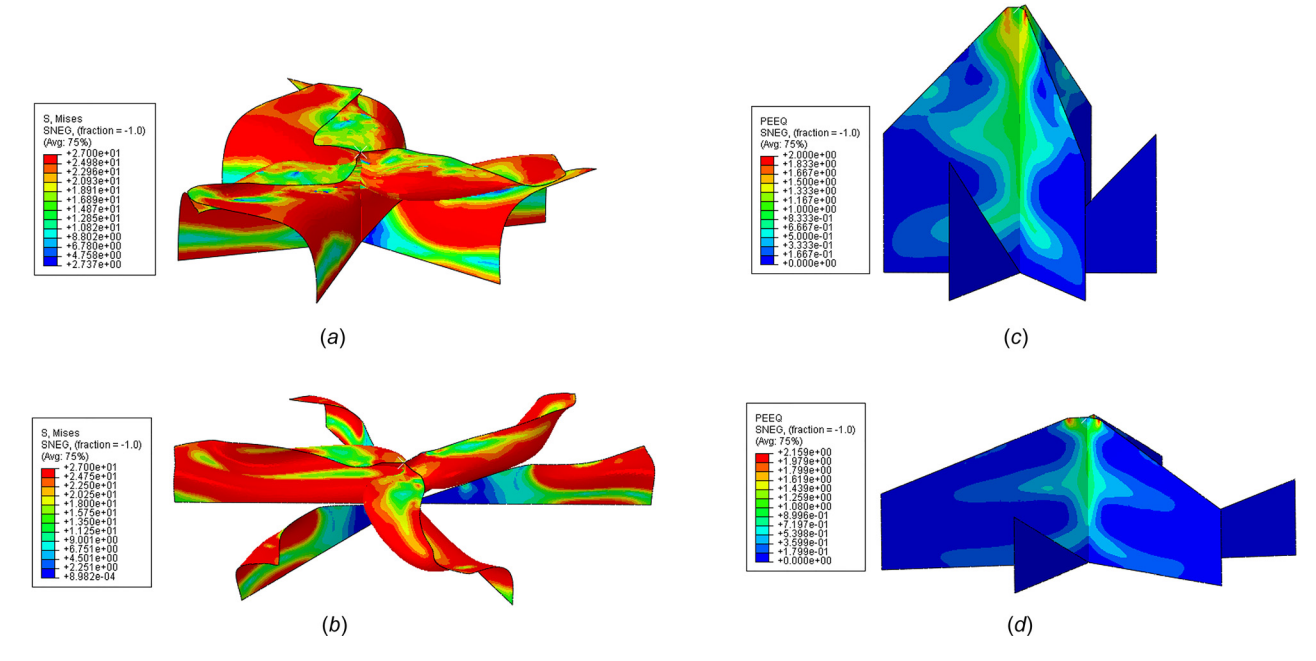


Fig. 8 (a) and (b) Mises stress maps of No. 1 and No. 3 models on deformed shapes. (c) and (d) PEEQ contour maps of No. 1 and No. 3 models on undeformed shapes. Here, No. 1 and No. 3 models represent models with different I and In ratios shown in Table 1.

also explains that for l/h = 1, the initial buckling occurs later than that for l/h = 3. For the same reason, the effective stroke for l/h = 1 is smaller than that for l/h = 3, as shown in Table 1. Overall, smaller l/h ratio provides higher energy absorption efficiency (Table 1).

Figure 8 further shows the deformation characteristics for l/h=1 and 3. As seen in Fig. 8(a) for l/h=1, in addition to the two plastic hinge lines as observed in Fig. 4 for l/h=1.81, the neighboring thin walls have contacted, and thus, provide another way to absorb energy, which is not observed for l/h=3 (Fig. 8(b)). This is also because the structure with l/h=1 is relatively denser than that for l/h=3. This self-compression for l/h=1 leads to smaller effective stroke, compared with individual folding in each thin wall structure for l/h=3, as summarized in Table 1. Figures 8(c) and 8(d) show that the plastic zone for l/h=1 is much larger than that for l/h=3.

To compare with a widely used energy absorber structure, namely a honeycomb structure, Fig. 7 and Table 1 also provide the results for honeycomb. The honeycomb specimen is fabricated using the same way of the origami models. To keep the same volume, same height, same cross-sectional area, and the same relative density as the origami absorber (l/h=1.81) described in experiment, a different wall thickness (t = 1.5 mm) is used. As shown in Fig. 7, honeycomb and origami-based structures show different characteristics. For honeycomb, the load first increases linearly during the elastic stage, resulting in a sharp peak of the load. Afterward, a valley of the load forms and the load finally increases at the densification stage. The major energy is absorbed at the primary stage due to the high peak force. Compared with the honeycomb structures, though the Ron Resch origami-inspired structures have lower energy absorption efficiency, the smaller peak force and the larger effective stroke offer unique characteristics as energy absorption structures. In other words, the Ron Resch origami-inspired and the classical honeycomb structures are complementary.

## 6 Conclusions

In this work, a novel energy absorbing structure inspired by the Ron Resch origami pattern is designed and investigated via both experiment and simulation. 3D printing method is used for fabricating the origami absorber and quasi-static axial crushing test is carried out for validating the energy absorbing properties. The results show a new collapse mode in terms of energy absorption featuring multiple plastic hinge lines, which lead to the peak force reduction and larger effective stroke, as compared with the classical honeycomb structure. Overall, the Ron Resch origami-inspired structure and the classical honeycomb structure are quite complementary as energy absorption structures.

### Acknowledgment

This work is supported by the National Natural Science Foundation of China and the Fundamental Research Funds for the Central Universities. H.J. acknowledges the support from the National Science Foundation.

## **Funding Data**

- National Natural Science Foundation of China (11525210, 11621062, and 91748209).
- National Science Foundation (CMMI-1762792).

#### References

- Hou, S. J., 2008, "Multiobjective Optimization of Multi-Cell Sections for the Crashworthiness Design," Int. J. Impact Eng., 35(11), pp. 1355–1367.
- [2] Fang, H., 2005, "Numerical Simulations of Multiple Vehicle Crashes and Multidisciplinary Crashworthiness Optimization," Int. J. Crashworthiness, 10(2), pp. 161–172.
- [3] Johnson, W., and Walton, A. C., 1983, "Protection of Car Occupants in Frontal Impacts With Heavy Lorries: Frontal Structures," Int. J. Impact Eng., 1(2), pp. 111–123.
- [4] Alghamdi, A. A. A., 2001, "Collapsible Impact Energy Absorbers: An Overview," Thin-Walled Struct., 39(2), pp. 189–213.
- [5] Sun, G. Y., 2011, "Crashworthiness Design of Vehicle by Using Multiobjective Robust Optimization," Struct. Multidiscip. Optim., 44(1), pp. 99–110.
- [6] Reid, J. D., and Sicking, D. L., 1998, "Design and Simulation of a Sequential Kinking Guardrail Terminal," Int. J. Impact Eng., 21(9), pp. 761–772.
- [7] Kanae, Y., Sasaki, T., and Shimamura, S., 1984, "Experimental and Analytical Studies on the Drop-Impact Test With Lead-Shielded Scale Model Radioactive Material Shipping Casks," Structural Impact and Crashworthiness, Vol. 2, Elsevier, New York.
- [8] Alghamdi, A. A. A., 2000, "Protection of Saudi Descent Roads Using Metallic Collapsible Energy Absorbers," KACST, Riyadh, Saudi Arabia, p. 74, Final Report No. 98-2-74.

- [9] Fairbairn, W., 1849, An Account of the Construction of the Britannia and Conway Tubular Bridges, John Weale, London.
- [10] Bryan, G. H., 1891, "On the Buckling of Simply Supported Rectangular Plates
- Uniformly Compressed in One Direction," Proc. London Math. Soc., 22, p. 54.
  [11] Alexander, J. M., 1960, "An Approximate Analysis of the Collapse of Thin Cylindrical Shells Under Axial Loading," Q. J. Mech. Appl. Math., 13(1), pp. 10-15.
- [12] Wierzbicki, T., and Abramowicz, W., 1983, "On the Crushing Mechanics of Thin-Walled Structures," ASME J. Appl. Mech., **50**(4a), pp. 727–734. [13] Abramowicz, W., and Jones, N., 1984, "Dynamic Axial Crushing of Square
- Tubes," Int. J. Impact Eng., 2(2), pp. 179–208.

  [14] Abramowicz, W., 1983, "The Effective Crushing Distance in Axially Com-
- pressed Thin-Walled Metal Columns," Int. J. Impact Eng., 1(3), pp.
- [15] Wierzbicki, T., and Abromowics, W., 1981, "Crushing of Thin-Walled Strain Rate Sensitive Structures," Eng. Trans., 29(1), pp. 153-163.
- [16] Umeda, T., 2010, "Study of Energy Absorption Efficiency for a Few Thin-Walled Tubes in Axial Crushing," J. Solid Mech. Mater. Eng., 4(7), pp. 875-890.
- [17] Mahdi, E., and Sebaey, T. A., 2014, "Crushing Behavior of Hybrid Hexagonal/ Octagonal Cellular Composite System: Aramid/Carbon Hybrid Composite," Mater. Des., 63, pp. 6-13.
- [18] Fan, Z., 2013, "Quasi-Static Axial Compression of Thin-Walled Tubes With Different Cross-Sectional Shapes," Eng. Struct., 55, pp. 80-89.
- [19] Ma, J., Le, Y., and You, Z., 2010, "Axial Crushing Tests of Steel Thin-Walled Square Tubes With Pyramid Pattern," AIAA Paper No. 2010-2615.
- [20] Ma, J., and You, Z., 2014, "Energy Absorption of Thin-Walled Square Tubes With a Prefolded Origami Pattern-Part I: Geometry and Numerical Simu-
- lation," ASME J. Appl. Mech., 81(1), p. 011003.
  [21] Zhou, C. H., 2017, "Crashworthiness Design for Trapezoid Origami Crash Boxes," Thin-Walled Struct., 117, pp. 257–267.
  [22] Giglio, M., 2012, "Investigations on Sandwich Core Properties Through an
- Experimental-Numerical Approach," Compos. Part B, 43(2), pp. 361-374.
- [23] Ivanez, I., 2010, "FEM Analysis of Dynamic Flexural Behaviour of Composite Sandwich Beams With Foam Core," Compos. Struct., 92(9), pp. 2285-2291.
- [24] Sanchez-Saez, S., 2015, "Dynamic Crushing Behaviour of Agglomerated Cork," Mater. Des., **65**, pp. 743–748.

- [25] Xiang, Y. F., 2016, "Comparative Analysis of Energy Absorption Capacity of Polygonal Tubes, Multi-Cell Tubes and Honeycombs by Utilizing Key Per-
- formance Indicators," Mater. Des., **89**, pp. 689–696.
  [26] Zhang, X., Cheng, G., and You, Z., 2007, "Energy Absorption of Axially Compressed Thin-Walled Square Tubes With Patterns," Thin-Walled Struct., **45**(9), pp. 737–746.
- [27] Adachi, T., 2008, "Energy Absorption of a Thin-Walled Cylinder With Ribs
- Subjected to Axial Impact," Int. J. Impact Eng., 35(2), pp. 65–79. [28] Song, J., 2012, "Axial Crushing of Thin-Walled Structures With Origami Patterns," Thin-Walled Struct., **54**, pp. 65–71.
- [29] Ma, J. Y., 2016, "Quasi-Static Axial Crushing of Thin-Walled Tubes With a Kite-Shape Rigid Origami Pattern: Numerical Simulation," Thin-Walled Struct., 100, pp. 38-47.
- [30] Yang, K., 2016, "Energy Absorption of Thin-Walled Tubes With Pre-Folded Origami Patterns: Numerical Simulation and Experimental Verification," Thin-Walled Struct., 103, pp. 33-44
- [31] Li, S., 2016, "Recoverable and Programmable Collapse From Folding Pressurized Origami Cellular Solids," Phys. Rev. Lett., 117(11), p. 114301.
- [32] Wang, B., and Zhou, C., 2017, "The Imperfection-Sensitivity of Origami Crash Boxes," Int. J. Mech. Sci., 121, pp. 58-66.
- [33] Zhou, C., and Wang, B., 2017, "Origami Crash Boxes Subjected to Dynamic Oblique Loading," ASME J. Appl. Mech., 84(9), p. 091006. Wang, F., and Chen, C., 2017, "Patterning Curved Three-Dimensional Structures
- With Programmable Kirigami Designs," ASME J. Appl. Mech., 84(6), p. 061007.
- [35] Safsten, G., Fillmore, T., Logan, A., Halverson, D., and Howell, L., 2016, "Analyzing the Stability Properties of Kaleidocycles," ASME J. Appl. Mech., 83(5), p. 051001.
- [36] Wang, W., and Qiu, X., 2017, "Coupling of Creases and Shells," ASME J. Appl. Mech., 85(1), p. 011009.
- [37] Lv, C., and Jiang, H., 2014, "Origami Based Mechanical Metamaterials," Sci. Rep., 4(1), p. 5979.
- [38] Che, K., and Meaud, J., 2016, "Three-Dimensional-Printed Multistable Mechanical Metamaterials With a Deterministic Deformation Sequence,"
- ASME J. Appl. Mech., 84(1), p. 011004.
  [39] Hanna, B. H., 2015, "Force–Deflection Modeling for Generalized Origami Waterbomb-Base Mechanisms," ASME J. Appl. Mech., 82(8), p. 081001.
- [40] Gardner, J. P., 2006, "The James Webb Space Telescope," Space Sci. Rev., 123(4), pp. 485-606.